Journal of the Brazilian Society of Mechanical Sciences and Engineering (2024) 46:588
https://doi.org/10.1007/s40430-024-05140-1

TECHNICAL PAPER

A comparative study of the predictive capability of multiaxial stress-based fatigue criteria

Thiago Abreu Peixoto[1] · Tiago Lima Castro[2] · Marcos Venicius Pereira[1] · Fathi Aref Darwish[3] · Bruno Felix de Carvalho[1]

Received: 9 May 2023 / Accepted: 13 July 2024

Abstract

A comparative study is made of the predictive capability of a number of critical plane-based criteria, namely Findley (F), Matake (M), Susmel & Lazzarin (S&L), Carpinteri & Spagnoli (C&S) and Liu & Mahadevan (L&M), as well as a mesoscopic scale-based model proposed by Papadopoulos (P). Such criteria were applied to a set of published loading conditions which correspond to fatigue resistance limits involving synchronous sinusoidal in-phase and out-of-phase bending and torsion. The predictive capabilities associated with the application of these models were evaluated based on the respective error indices, which measure the deviation of such predictions with respect to their experimentally observed values within an infinite-life context. Assessment of the overall predictive capability, involving the totality of the 65 loading conditions considered in this work, is then presented in the form of frequency histograms, exhibiting the dispersion of the error index for each of the criteria in question. Accordingly, one could verify that the predictive capability of the Papadopoulos criterion is generally superior to those corresponding to the critical plane-based models involved in this study. Finally, the influence of specific loading parameters such as mean normal stress and mean shear stress on the degree of dispersion in the frequency histograms is presented and discussed.

Keywords Fatigue resistance limits · Combined synchronous bending and torsion · Mean normal stress · Mean shear stress · Error index dispersion · Frequency histograms

Technical Editor: Santosh Kapuria.

✉ Thiago Abreu Peixoto
tapeixoto@yahoo.com.br

Tiago Lima Castro
tiagocastrobl@gmail.com

Marcos Venicius Pereira
marcospe@puc-rio.br

Fathi Aref Darwish
fadarwish-agouza@outlook.com

Bruno Felix de Carvalho
brunofelixcarvalho96@gmail.com

[1] Department of Chemical and Materials Engineering, Pontifical Catholic University of Rio de Janeiro – PUC-Rio, Rua Marquês de São Vicente, 225, Rio de Janeiro, RJ 22451-900, Brazil

[2] Department of Metallurgical and Materials Engineering, Federal University of Rio de Janeiro – UFRJ, Avenida Horário Macedo, 2030, Rio de Janeiro, RJ 21941-598, Brazil

[3] Department of Civil Engineering, Fluminense Federal University – UFF, Rua Passo da Pátria 156, Niterói, RJ 24210-240, Brazil

1 Introduction

The assessment of multiaxial high cycle fatigue behavior of metallic materials within an infinite-life context has been investigated for many years [1]. The main purpose of the investigations undertaken in several works has been to introduce relevant criteria capable of predicting whether or not fatigue failure would take place under given loading conditions. Among the many criteria encountered in the literature [2–10], stress-based models are the ones most popularly used for this purpose [11]. Accordingly, the present work has been initiated with the purpose of evaluating the capacity of a number of stress-based criteria to predict fatigue failure.

The selected criteria, which belong to two distinguished categories, namely critical plane-based and mesoscopic scale-based, were applied to a number of published loading conditions corresponding to fatigue resistance limits, involving synchronous sinusoidal in-phase and out-of-phase bending and torsion [12–14]. The assessment of the predictive capability, which is conducted based on analyzing the

Published online: 04 September 2024

dispersion of error indices relative to each criterion, was divided into two parts. After a first and broader analysis, which was carried out with the purpose of assessing the overall behavior of the models, a second and more specific investigation was conducted focusing on identifying the influence of certain loading parameters such as phase difference and the applied mean stresses on the predictive capability of each of the models in question.

The critical plane-based criteria considered in the study correspond to Findley (F), Matake (M), Susmel & Lazzarin (S&L), Carpinteri & Spagnoli (C&S) and Liu & Mahadevan (L&M). In addition to those, a mesoscopic scale-based criterion proposed by Papadopoulos (P) was also taken into consideration. The expressions representative of the aforementioned criteria are, respectively, given by [2–7]

$$C_a + kN_{\max} \leq f* \tag{1}$$

$$C_a + \mu N_{\max} \leq t_{-1} \tag{2}$$

$$C_a + k' \frac{N_{\max}}{C_a} \leq t_{-1} \tag{3}$$

$$\sqrt{N_{\max}^2 + \left(\frac{f_{-1}}{t_{-1}}\right)^2 C_a^2} \leq f_{-1} \tag{4}$$

$$\sqrt{\left[\frac{N_a\left(1+\eta\frac{N_m}{f_{-1}}\right)}{f_{-1}}\right]^2 + \left(\frac{C_a}{t_{-1}}\right)^2} \leq \lambda \tag{5}$$

$$\sqrt{\left(\frac{\sigma_a^2}{3} + \tau_a^2\right)} + \alpha\left(\frac{\sigma_a+\sigma_m}{3}\right) \leq t_{-1}. \tag{6}$$

In the above expressions, C_a corresponds to the shear stress amplitude and $N_{\max}$ to the maximum value attained by the normal stress within a loading cycle, both acting on the critical plane. The determination of such quantities is detailed in Sect. 2.1 of the present work, where the corresponding analytical expressions are presented.

The constants k, $f*$, μ, k', η and λ are, in turn, material parameters which are exclusively dependent on the fatigue resistance limits for fully reversed bending f_{-1} and fully reversed torsion t_{-1} [2–6], and their expressions are presented in Table 1. As for expression (6), σ_a and τ_a refer to the applied normal and shear stress amplitudes, while σ_m corresponds to the applied mean normal stress. Finally, α is a constant which is also a material parameter that, likewise, is exclusively dependent on f_{-1} and t_{-1} [7]. The expression of α is also presented in Table 1, along with the other aforementioned material parameters.

According to Carpinteri et al. [15], $N_{\max}$ in expression (4) can be replaced by the parameter $N_{a,eq}$ defined by

Table 1 Definition of pertinent material constants

$k = \frac{2-\left(\frac{f_{-1}}{t_{-1}}\right)}{2\sqrt{\left(\frac{f_{-1}}{t_{-1}}-1\right)}}$
$f* = \sqrt{\frac{f_{-1}^2}{4\left(\frac{f_{-1}}{t_{-1}}-1\right)}}$
$\mu = 2\left(\frac{t_{-1}}{f_{-1}}\right) - 1$
$k' = t_{-1} - \frac{f_{-1}}{2}$
$s = \frac{t_{-1}}{f_{-1}}$
$\eta = \frac{3}{4} + \frac{1}{4}\left(\frac{\sqrt{3}-\frac{f_{-1}}{t_{-1}}}{\sqrt{3}-1}\right)$
$\lambda = \left[\cos^2(2\delta)s^2 + \sin^2(2\delta)\right]^{1/2}$
$\alpha = \left(\frac{3t_{-1}}{f_{-1}}\right) - \sqrt{3}$

δ is given by expressions (19) and (20) for the C&S and L&M models, respectively

$$N_{a,eq} = N_a + f_{-1}\left(\frac{N_m}{\sigma_u}\right), \tag{7}$$

where σ_u is the ultimate tensile strength, giving rise to a modified version of the C&S criterion.

At this point, it is important to mention that the left-hand side (LHS) of expressions (1)–(6) refers to the driving force for fatigue failure, whereas the right-hand side (RHS) is associated with the fatigue resistance limit of the material. It follows that the comparison between the two sides of each expression would indicate whether or not fatigue failure is likely to occur. Accordingly, the error index, which represents a measure of the difference between the two sides, indicates whether the driving force exceeds the material's fatigue resistance. Another important observation refers to the fact that the criteria in question are applicable to hard metallic materials where the ratio t_{-1}/f_{-1} lies between $1/\sqrt{3}$ and 0.8 [2–7, 15].

2 Methods

As mentioned earlier, the selected criteria were applied to a set of loading conditions which correspond to experimentally observed fatigue resistance limits. For a given loading condition, the corresponding error index can be calculated by comparing the two sides of expressions (1)–(6). However, in order to apply the critical plane-based criteria presented in expressions (1)–(5), one must first determine the values of C_a and $N_{\max}$, which depend on critical plane orientation. In this section, a brief review on the stresses acting on a generic material plane within a specimen is carried out, followed by the presentation of the models' definitions of

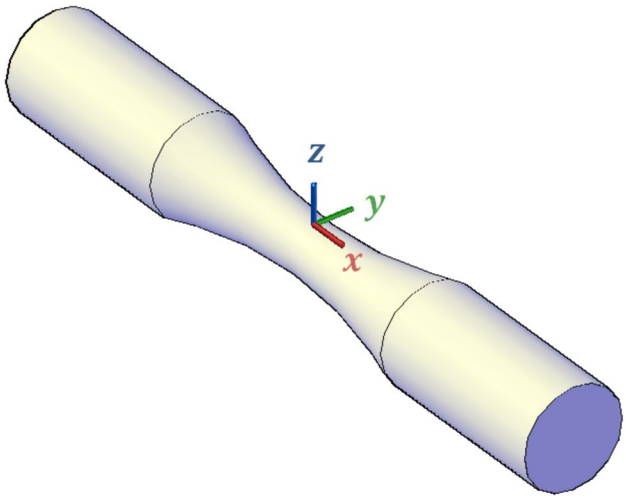

Fig. 1 Hourglass specimen with reference system positioned on the free surface, where the cross-sectional area is minimum (x-axis aligned with longitudinal direction of the specimen)

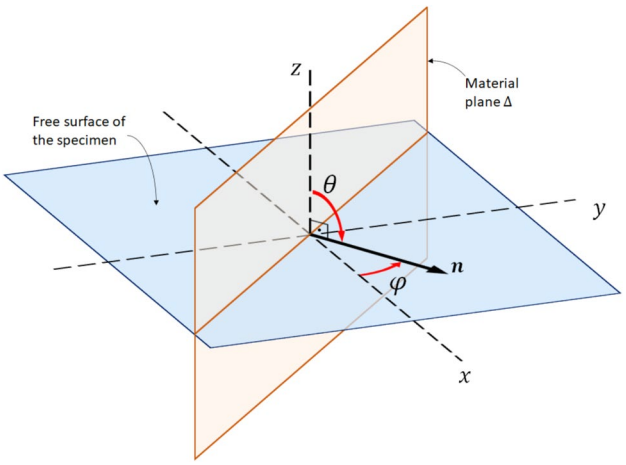

Fig. 2 Orientation of the material plane Δ determined by its unit normal vector $\boldsymbol{n}$ relative to the elementary area located at the free surface of the specimen, indicating the angles (θ, φ)

critical plane as well as the procedures for determining its orientation. Finally, the definition of error index is presented and its application on assessing the predictive capability of the models is discussed for the case of the 65 critical loading conditions extracted from the literature.

2.1 Stresses acting on a generic material plane

The procedure to determine the stresses acting on any given material plane is summarized here for the case of combined synchronous sinusoidal normal and shear stresses. The reference system, as positioned on the free surface of a specimen, is presented in Fig. 1 with the x-axis aligned with its longitudinal direction. The stress state associated with a combined bending and torsion loading is thus given by [7]

$$\sigma(t) = \begin{pmatrix} \sigma_{xx}(t) & \tau_{xy}(t) & 0 \\ \tau_{xy}(t) & 0 & 0 \\ 0 & 0 & 0 \end{pmatrix}, \tag{8}$$

where [7]

$$\sigma_{xx}(t) = \sigma_m + \sigma_a \sin(\omega t) \tag{9}$$

$$\tau_{xy}(t) = \tau_m + \tau_a \sin(\omega t - \beta), \tag{10}$$

with σ_a and τ_a representing, respectively, the applied normal and shear stress amplitudes and σ_m and τ_m, the corresponding mean stresses. The parameter β is the phase difference between the sinusoidal normal and shear stresses, while ω corresponds to the angular frequency of the cyclic loading. The notation adopted in expressions (8)–(10) indicates that the shear stress is delayed of β with respect to the normal stress loading.

Each material plane Δ intercepting the specimen can be uniquely determined by its unit normal vector $\boldsymbol{n}$, described in spherical coordinates in terms of the azimuthal and polar angles θ and φ. The former is the angle established between the normal vector $\boldsymbol{n}$ and the z-axis while the latter is the angle between the x-axis and the projection of $\boldsymbol{n}$ onto the xy-plane. This situation is illustrated in Fig. 2 where θ is equivalent to $\pi/2$.

As one would expect, the stresses acting on each material plane are dependent on the plane's orientation. Considering that the quantities σ_a, τ_a, σ_m, τ_m and β are known, the stresses acting on a material plane can thus be fully determined. The normal stress amplitude N_a and the mean normal stress N_m are given by [7]

$$N_a = \sin^2(\theta)|\cos(\varphi)|\sqrt{\sigma_a^2\cos^2(\varphi) + 4\tau_a^2\sin^2(\varphi) + 2\sigma_a\tau_a\sin(2\varphi)\cos(\beta)} \tag{11}$$

$$N_m = \sin^2(\theta)\left[\sigma_m\cos^2(\varphi) + \tau_m\sin(2\varphi)\right]. \tag{12}$$

As such, the maximum value attained by the normal stress within a loading cycle acting on the material plane Δ is therefore given by

$$N_{\max} = N_a + N_m. \tag{13}$$

Considering the case of synchronous normal and shear stress loadings described in expressions (8)–(10), the shear stress amplitude—which is the other quantity of interest—can also be analytically evaluated, as given by [7]

$$C_a = \sqrt{\frac{f^2+g^2+p^2+q^2}{2} + \sqrt{\left(\frac{f^2+g^2+p^2+q^2}{2}\right)^2 - (fq-gp)^2}}, \quad (14)$$

where the functions f, g, p and q are given by

$$f = \sin(\theta)\left[-\frac{\sigma_a}{2}\sin(2\varphi) + \tau_a\cos(2\varphi)\cos(\beta)\right] \quad (15)$$

$$g = -\sin(\theta)\left[\tau_a\cos(2\varphi)\sin(\beta)\right] \quad (16)$$

$$p = -\frac{1}{2}\sin(2\theta)\left[\sigma_a\cos^2(\varphi) + \tau_a\sin(2\varphi)\cos(\beta)\right] \quad (17)$$

$$q = \frac{1}{2}\sin(2\theta)\left[\tau_a\sin(2\varphi)\sin(\beta)\right]. \quad (18)$$

For the case of combined normal and shear stress loadings (Fig. 3), the angle θ associated with critical plane orientation is equivalent to $\pi/2$ [5, 16], and the above expressions will be greatly simplified. Both applied stresses $\sigma_{xx}(t)$ and $\tau_{xy}(t)$ are indicated in Fig. 3, along with the stresses $N_{\max}$ and C_a acting on the material plane Δ.

The values associated with normal and shear stress acting on each material plane depend on the respective plane orientation. Accordingly, evaluation of C_a and $N_{\max}$ acting on the critical plane requires the determination of critical plane orientation φ_c, which is defined differently according to each model.

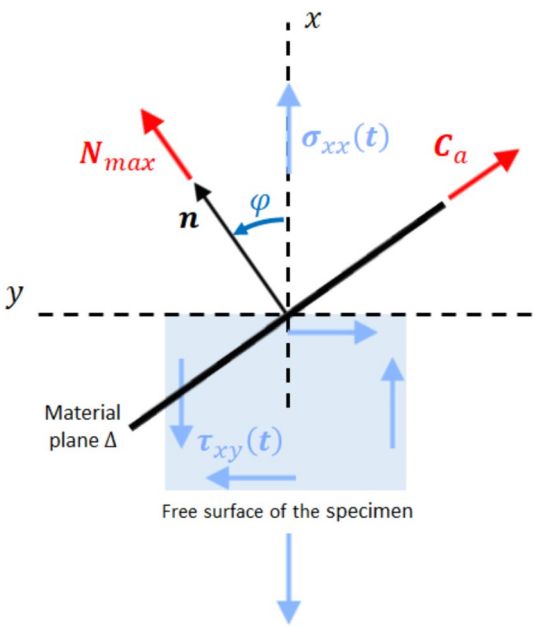

Fig. 3 Frontal view of the free surface of the specimen subjected to combined normal and shear stress cyclic loadings, where a given material plane Δ orientated at an angle φ experiences $N_{\max}$ and C_a

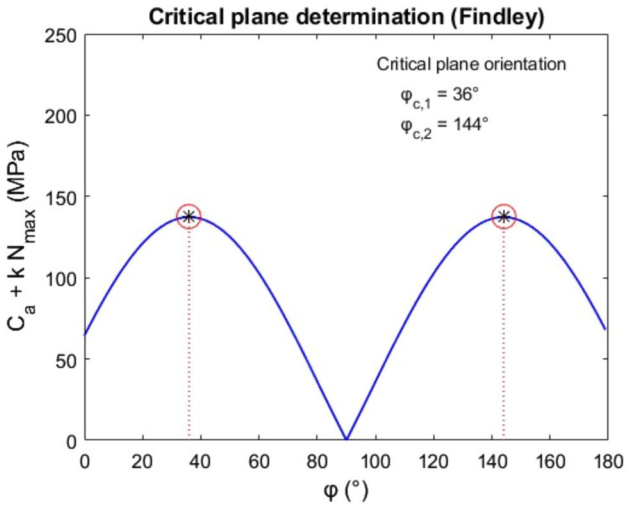

Fig. 4 Findley's critical plane determination procedure applied to the DIN 42CrMo4 steel for a pure push–pull stress amplitude of 200 MPa

Findley (F) considers that the material plane where the maximum value of the linear combination $C_a + kN_{\max}$ takes place as being the one that experiences the maximum damage due to fatigue. As such, critical plane can be directly obtained as the plane where Findley's fatigue parameter attains its maximum value, i.e., $\max\{C_a + kN_{\max}\}$, among all material planes within a given specimen [5, 7]. An example of Findley's critical plane determination procedure is provided in Fig. 4 for the case of a uniaxial push–pull (normal) stress amplitude of 200 MPa applied to a DIN 42CrMo4 specimen.

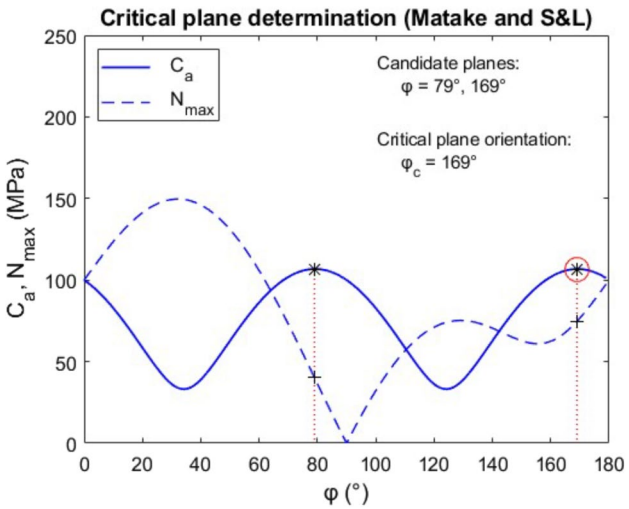

Fig. 5 Critical plane determination procedure for Matake and Susmel & Lazzarin applied to the DIN 42CrMo4 steel for combined normal and shear stress amplitudes of 100 MPa with a phase difference of 45°

As for Matake (M) and Susmel & Lazzarin (S&L), critical plane determination requires a two-step procedure. Given that the shear stress amplitude plays the most important role in fatigue damage, a set of candidate planes corresponding to those that experience the maximum shear stress amplitude C_a are preselected. The normal tensile stress, in turn, plays a secondary role as it tends to separate crack surfaces, abbreviating the life of the component in question. Consequently, the critical plane is the one where N_{max} attains its maximum value among a set of preselected candidate planes where the shear stress amplitude C_a had already been found to be maximum [2, 3, 5, 7]. Accordingly, as an example, Fig. 5 illustrates the critical plane determination procedure for the case of combined normal and shear stress amplitudes of 100 MPa applied to a DIN 42CrMo4 specimen, with a phase difference of 45°.

Regarding the C&S and L&M criteria, critical plane determination is based on knowing the fracture plane orientation φ_f as well as the angle δ established between fracture and critical planes. The fracture plane corresponds to the one on which the maximum normal stress $N_{\max}$ achieves its greatest value in the course of cyclic loading [5, 6, 15–17], as exemplified in Fig. 6a for a case of combined normal and shear stress amplitudes of 100 MPa applied to a DIN 42CrMo4 specimen, with a phase difference of 30°. The angle δ for the C&S and L&M criteria is, respectively, given by [5, 6]

$$\delta = \frac{3\pi}{8}\left[1 - \left(\frac{t_{-1}}{f_{-1}}\right)^2\right] \tag{19}$$

$$\delta = \frac{1}{2}\cos^{-1}\left[\frac{-2+\sqrt{4-4\left(\frac{1}{s^2}-3\right)\left(5-\frac{1}{s^2}-4s^2\right)}}{2\left(5-\frac{1}{s^2}-4s^2\right)}\right], \tag{20}$$

where s corresponds to the fatigue resistance limit ratio t_{-1}/f_{-1}. Once fracture plane orientation φ_f is known, critical plane orientation φ_c, as shown in Fig. 6b, will thus be given by

$$\varphi_c = \varphi_f + \delta, \tag{21}$$

where δ is defined by expressions (19) and (20) for C&S and L&M criteria, respectively.

In some cases, a second fracture plane orientation is revealed resulting in two fracture planes that are symmetrical with respect to the specimen's longitudinal direction. Their orientations are given by $\varphi_{f,1}$ and $\varphi_{f,2}$, which are supplementary angles. As such, critical plane orientation associated with $\varphi_{f,1}$ pertaining to the first quadrant is determined by $\varphi_{c,1} = \varphi_{f,1} + \delta$, as presented in Eq. (21). However, as $\varphi_{f,2}$ pertains to the second quadrant, determination of the second critical plane orientation takes the form $\varphi_{c,2} = \varphi_{f,2} - \delta$. The resulting critical planes are also symmetrical with respect to the longitudinal direction, as exemplified in Fig. 6c for a generic specimen, and the stresses acting on both critical planes are identical.

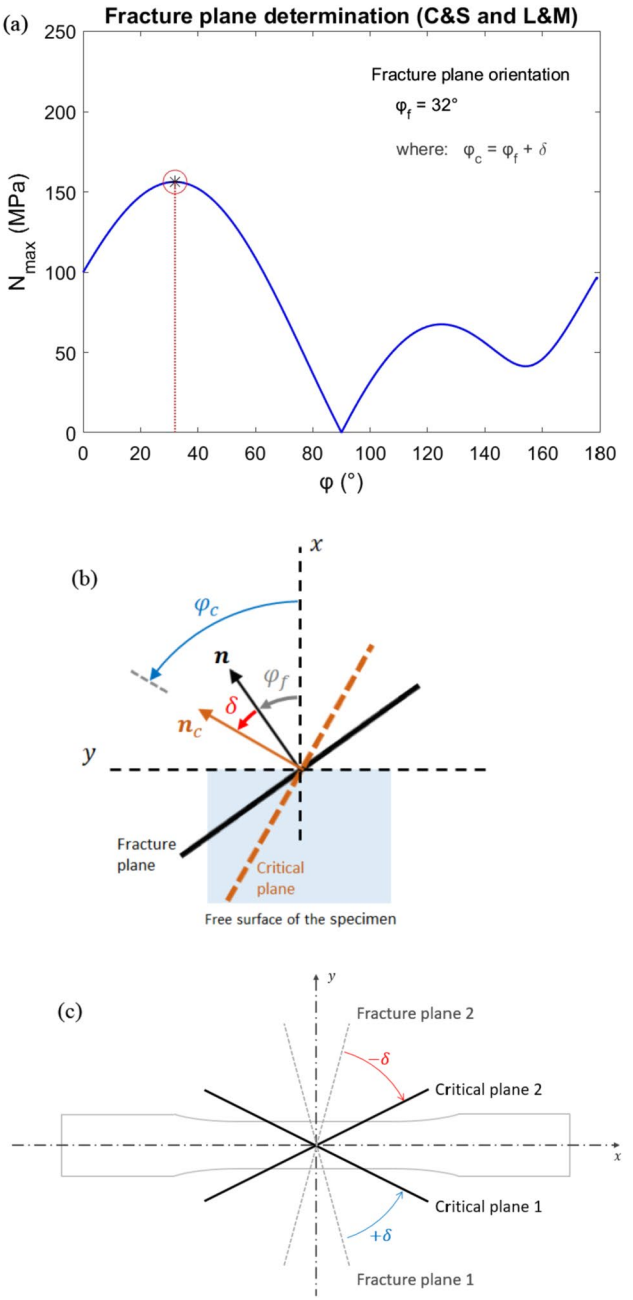

Fig. 6 Critical plane determination procedure for the C&S and L&M criteria applied to the DIN 42CrMO4 steel for combined normal and shear stress amplitudes of 100 MPa, with a phase difference of 30°: (**a**) identification of fracture plane; (**b**) determination of critical plane; (**c**) symmetrical orientations of fracture and critical planes

Finally, for all the involved critical plane-based models, inspection for critical plane orientation is carried out by enumeration, where C_a and $N_{\max}$ are evaluated as functions of φ, following incremental steps $\Delta\varphi$ of 0.1° in the interval

Table 2 Critical loading conditions, total of 65, relative to six different materials [5, 7]

	Loading conditions					
	#	$\sigma_a(MPa)$	$\sigma_m(MPa)$	$\tau_a(MPa)$	$\tau_m(MPa)$	$\beta(°)$
Swedish hard steel	1	327.7	0	0	0	0
	2	308	0	63.9	0	0
	3	255.1	0	127.5	0	0
	4	141.9	0	171.3	0	0
	5	0	0	201.1	0	0
	6	255.1	0	127.5	0	30
	7	142	0	171.2	0	30
	8	255.1	0	127.5	0	60
	9	147.2	0	177.6	0	60
	10	308	0	63.9	0	90
	11	264.9	0	132.4	0	90
	12	152.5	0	184.2	0	90
Hard steel	13	138.1	0	167.1	0	0
	14	140.4	0	169.9	0	30
	15	145.7	0	176.3	0	60
	16	150.2	0	181.7	0	90
	17	245.3	0	122.7	0	0
	18	249.7	0	124.9	0	30
	19	252.4	0	126.2	0	60
	20	258	0	129	0	90
	21	299.1	0	62.8	0	0
	22	304.5	0	63.9	0	90
42CrMo4	23	328	0	157	0	0
	24	286	0	137	0	90
	25	233	0	224	0	0
	26	213	0	205	0	90
	27	266	0	128	128	0
	28	283	0	136	136	90
	29	333	0	160	160	180
	30	280	280	134	0	0
	31	271	271	130	0	90
34Cr4	32	314	0	157	0	0
	33	315	0	158	0	60
	34	316	0	158	0	90
	35	315	0	158	0	120
	36	224	0	224	0	90
	37	380	0	95	0	90
	38	316	0	158	158	0
	39	314	0	157	157	60
	40	315	0	158	158	90
	41	279	279	140	0	0
	42	284	284	142	0	90
	43	355	0	89	178	0
	44	212	212	212	0	90
	45	129	0	258	0	90

Table 2 (continued)

	Loading conditions					
	#	$\sigma_a(MPa)$	$\sigma_m(MPa)$	$\tau_a(MPa)$	$\tau_m(MPa)$	$\beta(°)$
30NCD16	46	485	0	280	0	0
	47	480	0	277	0	90
	48	480	300	277	0	0
	49	480	300	277	0	45
	50	470	300	270	0	60
	51	473	300	273	0	90
	52	590	300	148	0	0
	53	565	300	141	0	45
	54	540	300	135	0	90
	55	211	300	365	0	0
Mild steel	56	245.3	0	0	0	0
	57	235.6	0	48.9	0	0
	58	187.3	0	93.6	0	0
	59	101.3	0	122.3	0	0
	60	0	0	142.3	0	0
	61	194.2	0	97.1	0	60
	62	108.9	0	131.5	0	60
	63	235.6	0	48.9	0	90
	64	208.1	0	104.1	0	90
	65	112.6	0	136	0	90

Table 3 Material properties

Material	$f_{-1}(MPa)$	$t_{-1}(MPa)$	$\sigma_u(MPa)$
Swedish hard steel	313.9	196.2	704.1
Hard steel	313.9	196.2	680
42CrMo4	398	260	1025
34Cr4	410	256	795
30NCD16	660	410	1880
Mild steel	235.4	137.3	518.8

Table 4 Material parameters relative to each material considered in the Findley, Matake, Susmel & Lazzarin and Carpinteri & Spagnoli criteria

	Findley		Matake	S&L	C&S
Material	k	$f*$	μ	k'	δ
Swedish hard steel	0.2583	202.64	0.2501	39.25	41.1295
Hard steel	0.2583	202.64	0.2501	39.25	41.1295
42CrMo4	0.3220	273.15	0.3065	61.00	38.6939
34Cr4	0.2569	264.31	0.2488	51.00	41.1842
30NCD16	0.2499	422.61	0.2424	80.00	41.4514
Mild steel	0.1689	139.24	0.1665	19.60	44.5368

Table 5 Material parameters relative to each material considered in the Liu & Mahadevan and Papadopoulos criteria

	L&M				P
Material	s	η	λ	δ	α
Swedish hard steel	0.6250	0.7951	0.9875	39.1666	0.1431
Hard steel	0.6250	0.7951	0.9875	39.1666	0.1431
42CrMo4	0.6533	0.8187	0.9758	36.6077	0.2277
34Cr4	0.6244	0.7946	0.9877	39.2318	0.1411
30NCD16	0.6212	0.7918	0.9890	39.5555	0.1316
Mild steel	0.5833	0.7560	0.9997	44.1421	0.0177

$0° \leq \varphi < 180°$, allowing one to identify the critical plane according to each model's definition.

2.2 Error index *I*

Considering that the LHS and RHS of expressions (1)–(6) are, respectively, associated with the driving force to failure and the material's fatigue resistance, the difference between LHS and RHS relative to a given criterion indicates whether or not fatigue failures are to be expected. Such difference can be evaluated using the error index I, defined as [5, 7]

Table 6 Fracture and critical plane φ_f and φ_c orientations occurring at θ corresponding to 90°

	Fracture planes		Critical planes									
			Findley				Matake/S&L		C&S/Modified C&S		L&M	
#	$\varphi_{f,1}(^\circ)$	$\varphi_{f,2}(^\circ)$	$\varphi_{c,1}(^\circ)$	$\varphi_{c,2}(^\circ)$	$\varphi_{c,3}(^\circ)$	$\varphi_{c,4}(^\circ)$	$\varphi_{c,1}(^\circ)$	$\varphi_{c,2}(^\circ)$	$\varphi_{c,1}(^\circ)$	$\varphi_{c,2}(^\circ)$	$\varphi_{c,1}(^\circ)$	$\varphi_{c,2}(^\circ)$
1	0	–	37.8	142.2	–	–	45	135	41.1	–	39.2	–
2	11.3	–	153.5	–	–	–	146.3	–	52.4	–	50.5	–
3	22.5	–	164.7	–	–	–	157.5	–	63.6	–	61.7	–
4	33.8	–	176	–	–	–	168.8	–	74.9	–	73	–
5	45	135	7.2	82.8	97.2	172.8	0	90	86.1	93.9	84.2	95.8
6	21.6	–	164.3	–	–	–	157.5	–	62.7	–	60.8	–
7	34.1	–	176.0	–	–	–	169.8	–	75.2	–	73.3	–
8	17.6	–	164.1	–	–	–	157.5	–	58.7	–	56.8	–
9	35.4	–	176.9	–	–	–	173.4	–	76.5	–	74.6	–
10	0	–	36.9	143.1	–	–	45	135	41.1	–	39.2	–
11	0	–	0	–	–	–	45	135	41.1	–	39.2	–
12	39	141	0	–	–	–	0	–	80.1	99.9	78.2	101.8
13	33.8	–	176	–	–	–	168.8	–	74.9	–	73	–
14	34.1	–	176.1	–	–	–	169.8	–	75.2	–	73.3	–
15	35.5	–	176.9	–	–	–	173.4	–	76.6	–	74.7	–
16	39.1	140.9	0	–	–	–	0	–	80.2	99.8	78.3	101.7
17	22.5	–	60.3	–	–	–	67.5	–	63.6	–	61.7	–
18	21.6	–	164.4	–	–	–	157.5	–	62.7	–	60.8	–
19	17.6	–	164.1	–	–	–	157.5	–	58.7	–	56.8	–
20	0	–	0	–	–	–	0	–	41.1	–	39.2	–
21	11.4	–	153.6	–	–	–	146.4	–	52.5	–	50.6	–
22	0	–	36.9	143.1	–	–	45	135	41.1	–	39.2	–
23	21.9	–	165.8	–	–	–	156.9	–	60.6	–	58.5	–
24	0	–	0	–	–	–	45	135	38.7	–	36.6	–
25	31.3	–	175.2	–	–	–	166.3	–	70	–	67.9	–
26	34.2	–	0	–	–	–	0	–	72.9	–	70.8	–
27	31.3	–	55.8	–	–	–	67	–	70	–	67.9	–
28	29	–	31.2	–	–	–	45	–	67.7	–	65.6	–
29	0	–	19	–	–	–	23.1	–	38.7	–	36.6	–
30	12.8	–	168.3	–	–	–	156.9	–	51.5	–	49.4	–
31	0	–	0	–	–	–	45	135	38.7	–	36.6	–
32	22.5	–	60.3	164.7	–	–	67.5	157.5	63.7	–	61.7	–
33	17.7	–	164.1	–	–	–	157.6	–	58.9	–	56.9	–
34	0	–	0	–	–	–	0	–	41.2	–	39.2	–
35	162.3	–	15.9	–	–	–	22.4	–	203.5	–	201.5	–
36	35.3	144.7	0	–	–	–	0	–	76.5	103.5	74.5	105.5
37	0	–	36.5	143.5	–	–	45	135	41.2	–	39.2	–
38	31.7	–	58.1	–	–	–	67.5	–	72.9	–	70.9	–
39	31.3	–	54.1	–	–	–	67.5	–	72.5	–	70.5	–
40	30.1	–	29.8	–	–	–	0	–	71.3	–	69.3	–
41	13.3	–	167	–	–	–	157.6	–	54.5	–	52.5	–
42	0	–	0	–	–	–	0	–	41.2	–	39.2	–
43	28.2	–	50	–	–	–	58.3	–	69.4	–	67.4	–
44	0	–	0	–	–	–	0	–	41.2	–	39.2	–
45	43.1	136.9	0	–	–	–	0	–	84.3	95.7	82.3	97.7
46	24.6	–	166.6	–	–	–	159.6	–	66.1	–	64.2	–
47	0	–	0	–	–	–	0	–	41.5	–	39.6	–

Table 6 (continued)

	Fracture planes		Critical planes									
			Findley				Matake/S&L		C&S/Modified C&S		L&M	
#	$\varphi_{f,1}(^\circ)$	$\varphi_{f,2}(^\circ)$	$\varphi_{c,1}(^\circ)$	$\varphi_{c,2}(^\circ)$	$\varphi_{c,3}(^\circ)$	$\varphi_{c,4}(^\circ)$	$\varphi_{c,1}(^\circ)$	$\varphi_{c,2}(^\circ)$	$\varphi_{c,1}(^\circ)$	$\varphi_{c,2}(^\circ)$	$\varphi_{c,1}(^\circ)$	$\varphi_{c,2}(^\circ)$
48	17.7	–	167.7	–	–	–	159.5	–	59.2	–	57.3	–
49	15.3	–	168	–	–	–	160.4	–	56.8	–	54.9	–
50	12.5	–	169	–	–	–	161.4	–	54	–	52.1	–
51	0	–	0	–	–	–	0	–	41.5	–	39.6	–
52	9.2	–	157.6	–	–	–	148.3	–	50.7	–	48.8	–
53	6.7	–	155.8	–	–	–	145.8	–	48.2	–	46.3	–
54	0	–	31.9	148.1	–	–	45	135	41.5	–	39.6	–
55	27.5	–	179	–	–	–	171.9	–	69	–	67.1	–
56	0	–	40.2	139.8	–	–	45	135	44.5	–	44.1	–
57	11.3	–	51.5	–	–	–	146.3	–	55.8	–	55.4	–
58	22.5	–	62.7	–	–	–	157.5	–	67	–	66.6	–
59	33.8	–	74	–	–	–	168.8	–	78.3	–	77.9	–
60	45	135	4.8	85.2	94.8	175.2	0	90	89.5	90.5	89.1	90.9
61	17.6	–	161.8	–	–	–	157.5	–	62.1	–	61.7	–
62	35.4	–	175.5	–	–	–	173.4	–	79.9	–	79.5	–
63	0	–	39.7	140.3	–	–	45	135	44.5	–	44.1	–
64	0	–	0	–	–	–	0	–	44.5	–	44.1	–
65	39	141	0	–	–	–	0	–	83.5	96.5	83.1	96.9

$$I = \frac{\text{LHS}-\text{RHS}}{\text{RHS}} \times 100\%. \tag{22}$$

As one may observe, positive I values correspond to a situation where the driving force to failure (LHS) exceeds the material's fatigue resistance (RHS), indicating that failure is expected to occur. Negative I values, in turn, correspond to a situation where the driving force is less than the material's fatigue resistance, meaning that fatigue cracks are not to be expected. Accordingly, when the LHS equals the RHS, it implies that the material has been driven to the verge of failure and the corresponding loading condition is therefore said to be critical. In this case, the error index I turns out to be nil.

2.3 Critical loading conditions

In order to assess their predictive capabilities, the selected stress-based criteria were applied to a set of critical loading conditions (total of 65) extracted from the literature [12–14], relative to six different metallic materials. Such loading conditions, corresponding to the limiting state of fracture/non-fracture for a number of load cycles in the order of one million [7], are presented in Table 2, while the materials' pertinent mechanical properties are exhibited in Table 3 [5, 7].

By applying the models to such loading conditions, a set of 65 error indices are thus revealed for each criterion. Given the critical nature of the involved loading conditions, models with good predictive capabilities tend to deliver a higher number of error indices close to zero. It is to be noted that positive I values indicate a conservative behavior of the model, as the criterion indicates the occurrence of failure for loading conditions that are known to be just critical. Analogously, negative I values correspond to a nonconservative behavior of the model, as the indication of non-fracture may inadequately suggest that the stress levels can be raised, thus increasing risk of fatigue failure.

The assessment of the predictive capabilities of the models consists of identifying the number of positive, nil and negative error indices delivered by each criterion, as well as the dispersion of error indices with the respect to the ideal I value corresponding to zero. The nature of a given model, whether it is conservative or nonconservative, can be determined by analyzing the error index dispersion. In addition, the statistics relative to the error index dispersions are obtained and the predictive capabilities of the models in question are discussed.

Table 7 Error indices for all the considered criteria relative to the 65 critical loading conditions

#	Error index I (%)						
	F	M	S&L	C&S	C&S (Mod)	L&M	P
1	4.4	4.4	3.5	1.8	1.8	4.4	4.4
2	4.6	4.6	3.5	1.2	1.2	3.8	3.8
3	8.2	8.2	6.1	3.1	3.1	5.4	5.5
4	3.5	3.6	2.2	−1.5	−1.5	0.0	0.2
5	2.5	2.5	2.5	1.9	1.9	2.5	2.5
6	6.9	7.5	5.6	0.2	0.2	2.4	5.5
7	3.4	4.5	2.9	−3.6	−3.6	−2.2	0.2
8	2.6	3.8	3.9	−7.7	−7.7	−5.7	5.5
9	6.8	9.3	7.0	−5.7	−5.7	−4.7	3.9
10	−0.2	−0.3	0.2	−2.2	−2.2	0.4	3.8
11	−0.9	−8.6	−4.2	−7.3	−7.3	−4.8	9.5
12	10.3	13.3	10.4	−8.5	−8.5	−8.3	7.8
13	1.0	1.0	−0.2	−4.0	−4.0	−2.5	−2.3
14	2.5	3.6	2.1	−4.4	−4.4	−3.0	−0.6
15	5.9	8.4	6.3	−6.4	−6.4	−5.4	3.1
16	8.8	11.8	9.1	−9.7	−9.7	−9.5	6.3
17	4.1	4.1	2.6	−0.8	−0.8	1.4	1.5
18	4.7	5.2	3.8	−1.9	−1.9	0.3	3.3
19	1.5	2.7	3.0	−8.6	−8.6	−6.7	4.4
20	−3.5	−1.4	5.8	−9.7	−9.7	−7.3	6.7
21	1.7	1.7	1.1	−1.6	−1.6	0.9	0.9
22	−1.3	−1.4	−0.7	−3.2	−3.2	−0.7	2.7
23	6.7	6.7	4.3	0.7	0.7	4.1	4.2
24	−16.1	−21.7	−12.5	−22.2	−22.2	−19.1	−9.1
25	10.8	10.9	8.0	4.1	4.1	7.0	7.3
26	0.2	4.0	3.2	−24.9	−24.9	−23.8	−1.8
27	0.5	−2.5	−0.4	−14.0	−20.5	−17.6	−15.3
28	−6.2	−6.4	9.5	−26.8	−36.0	−34.8	−10.0
29	18.8	22.0	17.4	−8.5	−19.4	−16.3	5.9
30	22.4	19.0	20.2	8.3	−4.6	1.9	−2.9
31	11.5	−9.8	8.1	7.2	−14.1	−8.0	−5.9
32	2.0	2.0	0.8	−2.7	−2.7	−0.6	−0.5
33	−2.9	−1.8	−0.4	−12.6	−12.6	−10.8	−0.1
34	−9.5	−7.6	1.6	−15.3	−15.3	−13.1	0.1
35	−2.9	−1.8	−0.4	−6.0	−6.0	−3.7	−0.1
36	6.5	9.3	7.4	−15.8	−15.8	−15.6	5.2
37	−5.0	−5.1	−3.5	−6.6	−6.6	−4.2	0.4
38	16.2	13.5	11.3	−0.7	−5.6	−4.2	0.1
39	3.9	−0.5	1.1	−11.4	−16.7	−16.4	−0.5
40	−0.5	−7.7	1.4	−21.8	−28.2	−29.4	−0.1
41	16.3	14.0	15.3	4.5	−3.5	−2.2	−6.4
42	8.9	10.7	35.2	6.9	−8.8	−8.5	−4.8
43	11.8	10.3	11.4	−10.3	−17.9	−17.4	−6.2
44	21.4	24.0	22.7	−2.0	−14.6	−12.9	3.4
45	10.1	13.3	10.7	−0.3	−0.3	0.1	7.3
46	4.7	4.7	3.2	−0.3	−0.3	1.7	1.8
47	−6.1	−4.1	1.4	−17.2	−17.2	−15.2	0.7
48	20.4	19.1	16.2	7.8	3.0	5.7	3.9
49	17.8	17.8	16.8	2.6	−3.2	−0.4	3.9

Table 7 (continued)

	Error index I (%)						
#	F	M	S&L	C&S	C&S (Mod)	L&M	P
50	13.4	13.7	15.9	−2.2	−9.4	−6.3	1.6
51	10.3	12.3	21.8	1.2	−11.9	−6.9	2.5
52	12.9	10.8	10.8	8.8	0.8	5.0	0.1
53	6.0	3.9	6.8	3.7	−5.4	−1.4	−4.1
54	−4.1	−7.4	−1.5	0.1	−11.7	−7.9	−8.1
55	16.6	16.3	13.2	−4.3	−6.1	−5.8	−0.7
56	4.2	4.2	3.6	3.8	3.8	4.2	4.2
57	7.2	7.2	6.1	5.9	5.9	6.3	6.3
58	7.8	7.8	6.5	4.7	4.7	5.0	5.0
59	2.6	2.6	1.9	−1.0	−1.0	−0.9	−0.8
60	3.6	3.6	3.6	3.6	3.6	3.6	3.6
61	3.5	4.1	3.9	−2.9	−2.9	−2.7	8.9
62	8.6	9.7	8.3	−0.5	−0.5	−0.5	6.6
63	1.3	1.3	1.3	1.9	1.9	2.2	6.3
64	0.0	1.1	4.4	−1.4	−1.4	−1.1	16.7
65	11.3	12.7	10.9	−2.2	−2.2	−2.3	10.3

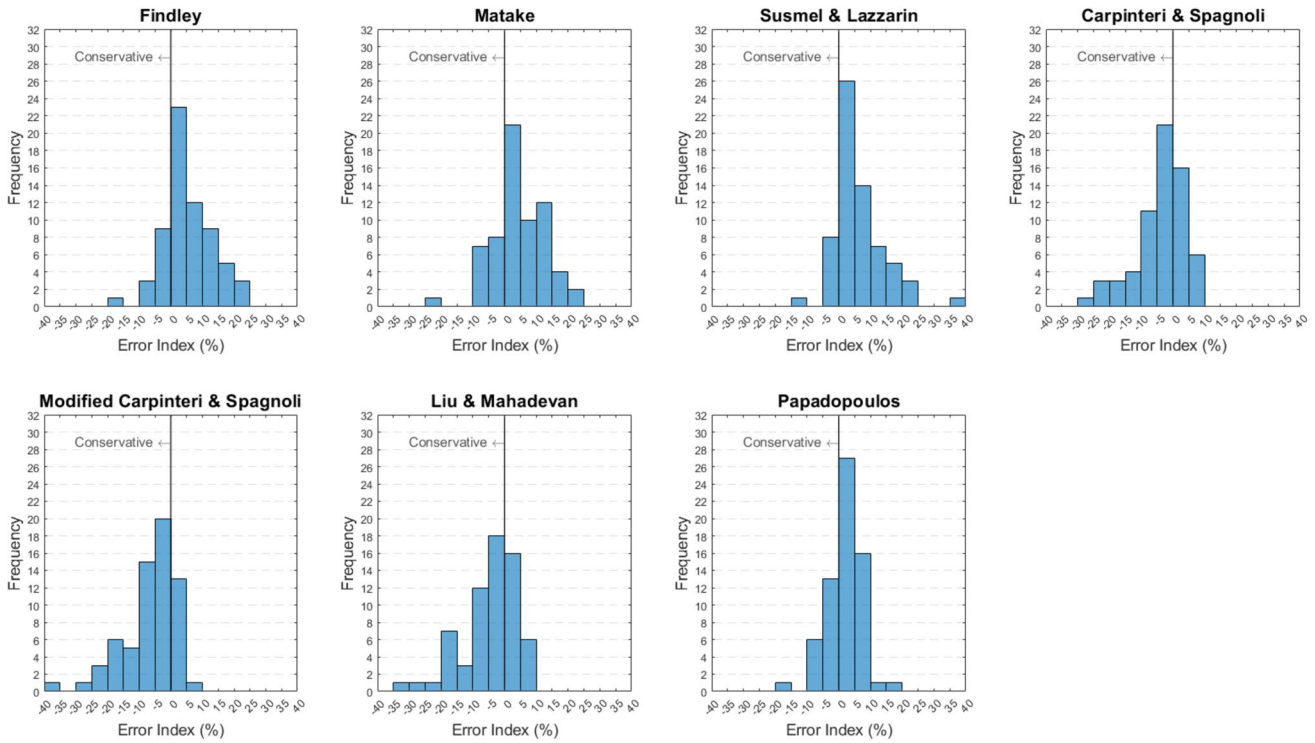

Fig. 7 Frequency histograms summarizing the error index dispersions

3 Results and discussion

3.1 Analyzing overall behaviors

The application of the selected stress-based criteria to the aforementioned critical loading conditions resulted in a set of 65 error indices for each of the involved models. The material parameters considered in the calculations are presented in Tables 4 and 5, while the resulting fracture

Table 8 Frequency histogram statistics

	Average	Std deviation	Min	Median	Max	Range
Findley, F	5.3	7.5	−16.1	4.4	22.4	38.5
Matake, M	5.0	8.3	−21.7	4.2	24.0	45.7
Susmel & Lazzarin, S&L	6.2	7.4	−12.5	3.9	35.2	47.7
Carpinteri & Spagnoli, C&S	−3.6	8.0	−26.8	−2.0	8.8	35.6
Modified C&S	−6.4	8.5	−36.0	−4.4	5.9	41.9
Liu & Mahadevan, L&M	−4.7	8.6	−34.8	−2.5	7.0	41.8
Papadopoulos, P	1.8	5.3	−15.3	2.5	16.7	32.0

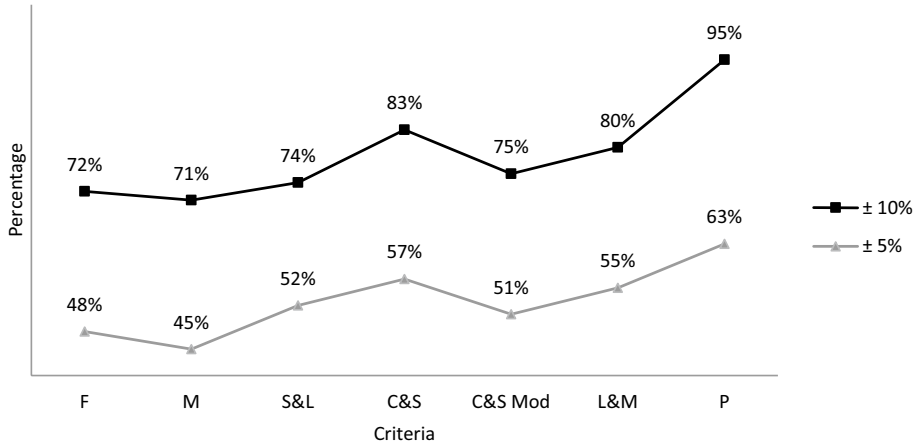

Fig. 8 Analyzing overall behavior: percentage of error indices pertaining to a central *I* range around 0%

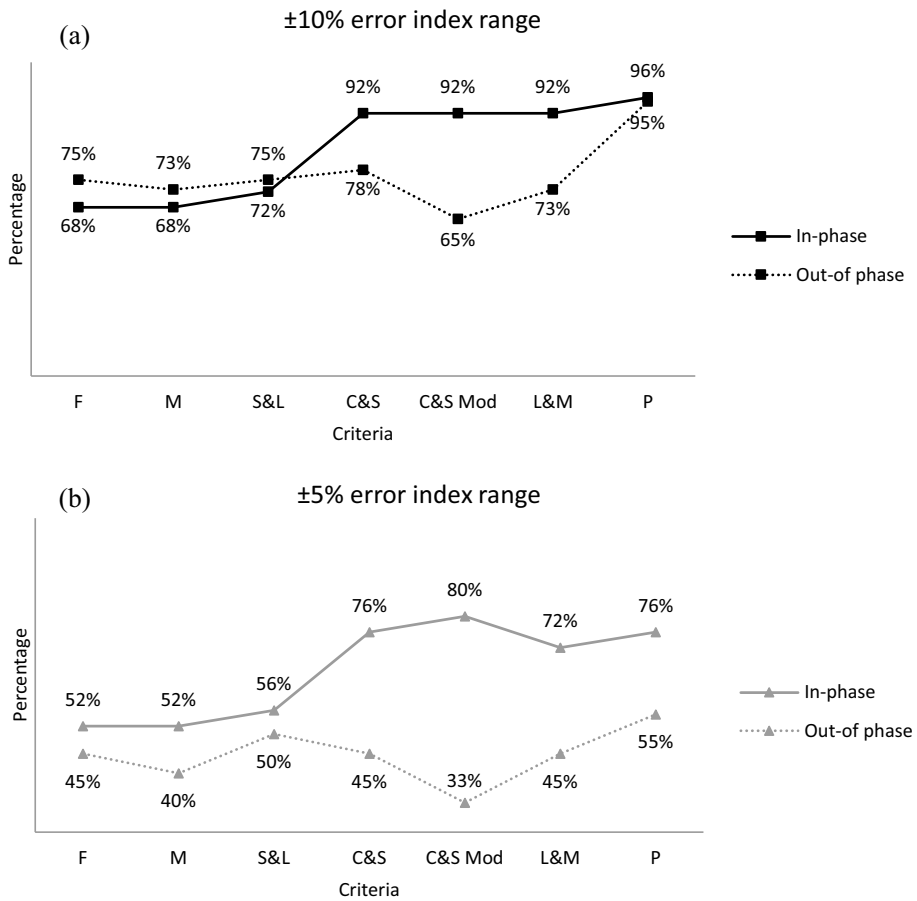

Fig. 9 Influence of phase difference on the comparative efficacy of the models

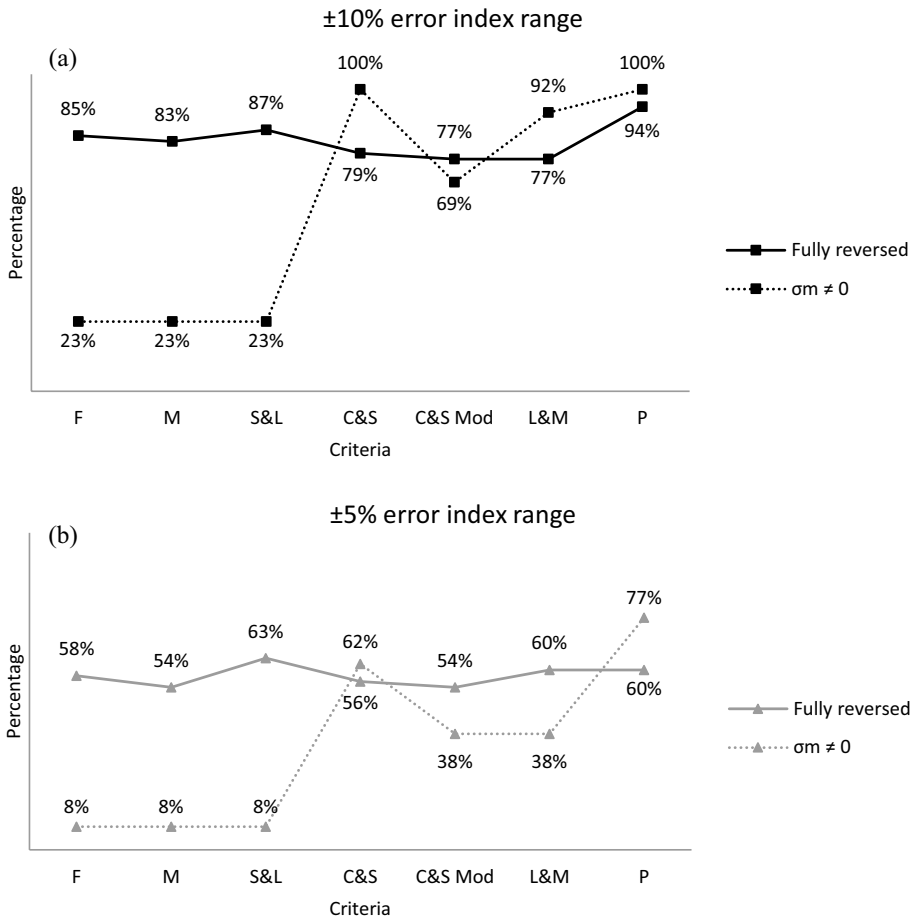

Fig. 10 Influence of mean normal stress σ_m on the comparative efficacy of the models

and critical planes (associated with the critical plane-based models) are exhibited in Table 6. Finally, the resulting error indices are presented in Table 7.

The dispersions of error indices are grouped and presented in Fig. 7 in the form of frequency histograms relative to the F, M, S&L, C&S, Modified C&S, L&M, and P criteria. The horizontal axis represents the values of error index divided into intervals of 5%. The number of occurrences relative to each histogram bin is represented by the vertical column above each interval.

Accordingly, an overall analysis of the predictive capabilities can be carried out by evaluating the statistics associated with each model's dispersion. The statistics presented in Table 8 have revealed that the S&L criterion presented I values between −12.5% and + 35.2%, corresponding to a range of 47.7%. This is followed in decreasing order by M, Modified C&S, L&M, F and C&S criteria, respectively, corresponding to 45.7%, 41.9%, 41.8%, 38.5% and 35.6%. Papadopoulos, in turn, revealed the lowest range among all, which corresponds to 32%.

Considering the 65 loading conditions in question, error indices delivered in the vicinity of zero indicate good predictive capability of the model in question. Accordingly, average values close to nil accompanied by low standard deviations can be interpreted as an indication of good overall performance of the criterion. In this sense, Papadopoulos presents the best error index average (1.8%), accompanied by the lowest standard deviation (5.3%) among all. Such a tendency can be graphically perceived in Fig. 7, where Papadopoulos' presents the most concise dispersion among all the considered models.

Nevertheless, statistics by themselves can be misleading, as low averages (in absolute values) may hide the fact that high positive error indices may cancel out with negative counterparts. Therefore, a good way to assess the predictive capability of a given model consists of identifying the number of occurrences of error indices within specific central ranges, such as ± 10% and ± 5%. As one would expect, the higher the number of occurrences within these central ranges, the better is the predictive capability of the criterion in question.

Figure 8 presents the percentage of occurrences within the intervals of ± 10% and ± 5% for all the involved criteria. As one may observe, Papadopoulos and C&S present the best overall behavior in both scenarios, where Papadopoulos, respectively, corresponded to 95% and 63% in the

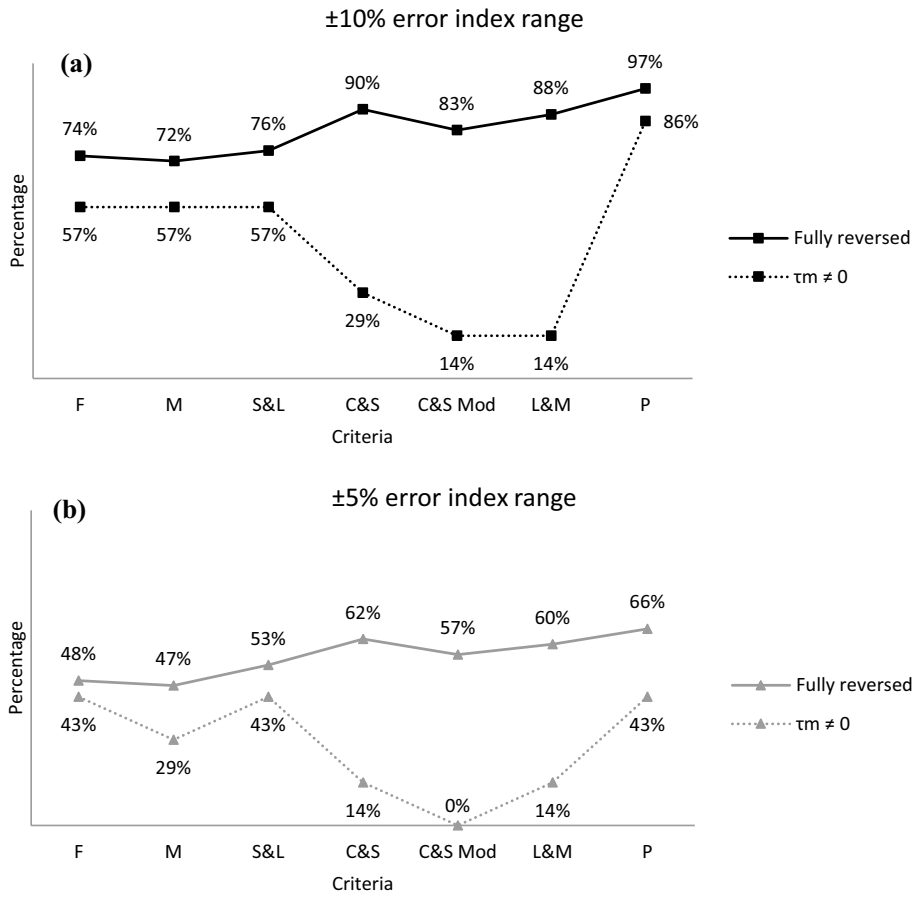

Fig. 11 Influence of mean shear stress τ_m on the comparative efficacy of the models

intervals of interest, while C&S, respectively, delivered 83% and 57% within the same ranges.

3.2 Influence of specific loading parameters

In an effort to delineate the influence of out-of-phase loading on the comparative efficacy of the criteria in question, the percentage of tests pertaining to a central I interval of $\pm 10\%$ is presented in Fig. 9a, in comparison with that corresponding to in-phase loading. Such a comparison is also presented, considering the central I range of $\pm 5\%$ shown in Fig. 9b. As Fig. 9 indicates, the efficacy expressed by the percentage of occurrences within the intervals referred to above is generally lower for the case of out-of-phase loading. However, it is noticeable that the efficacy of the Papadopoulos criterion is not significantly reduced as the applied loads become out-of-phase. In fact, almost no reduction is observed for the $\pm 10\%$ I interval, which is seen to be consistent with the reality of the criterion as being independent of whether the applied normal and torsion loads are in-phase or out-of-phase.

As to the effect of mean normal stress σ_m on the comparative efficacy of the models, the percentage of tests belonging to the central I ranges around 0% is presented in Fig. 10, in comparison with the percentage established for fully reversed normal loading. As illustrated in this figure, the percentage of tests belonging to the selected I intervals decrease in the case of the F, M and S&L criteria upon changing the applied loads from fully reversed to a situation where σ_m is not nil. A small reduction of 8% was also verified for the Modified C&S criterion. On the other hand, the efficacies of the C&S and P criteria are not negatively affected by the presence of mean normal stress. As to the F, M and S&L criteria, whose efficacy deteriorates significantly due to the introduction of a mean normal stress component, more non-fully reversed loading conditions should be considered in order to verify their behavior.

Finally, the influence of mean shear stress on the comparative predictive capability of the models is illustrated in Fig. 11, where the percentage of tests pertaining to the central I intervals is compared to that detected for fully reversed torsional loadings. In comparison with the F, M and S&L criteria, Fig. 11 indicates that Papadopoulos' is more precise in predicting fatigue behavior in the presence of mean shear stress, as it presents the smallest percent reduction among all the considered criteria. In regard to the C&S, Modified C&S and L&M criteria, the efficacy of the P criterion is seen to be far superior. Again, this is consistent with the formulation of

Papadopoulos' model, as it is conceived to be independent of mean shear stress.

4 Conclusions

Based on what is presented above, the following conclusions can be drawn:

- From an overall perspective, the dispersion of the error indices obtained for the critical plane-based models ranged from 47.7% for the S&L criterion to 35.6% in the case of the C&S. The other criteria presented dispersions which ranged between those mentioned above, namely 45.7%, 41.9%, 41.8% and 38.5%, respectively, for the Matake, Modified C&S, L&M and Findley criteria.
- The mesoscopic scale-based model proposed by Papadopoulos, when applied to the same critical loading conditions, revealed the most concise dispersion in terms of range among all, indicating higher consistency in its predictive capability.
- Papadopoulos' criterion presented the best overall average (1.8%) associated with the lowest standard deviation (5.3%) among all the models considered in this work, which is indicative of a good overall performance of the model.
- Regarding the number of occurrences of error indices within the $\pm$ 10% central interval, Papadopoulos' was seen to deliver 95% of its predictions within such interval, being higher than the numbers revealed for the critical plane-based models.
- From a more specific perspective, the overall performance of the critical plane-based models is generally reduced with the introduction of phase differences. On the other hand, it is to be noted that the predictive capability relative to the Papadopoulos criterion remained consistent and practically unaltered for out-of-phase loading conditions.
- Regarding the presence of a mean normal stress, it is revealed that such parameter exerted a negative influence upon the overall behavior of the F, M, S&L and Modified C&S, whereas the performances of the C&S and P criteria were not negatively affected.
- Finally, regarding the influence of the mean shear stress, the performance delivered by the Papadopoulos criterion was revealed to be considerably superior to those associated with critical plane-based models.

Acknowledgements This research was developed within the scope of the Research and Technological Development of the Brazilian Electric Energy Sector Program regulated by ANEEL, with the support of the Eneva Companies—Pecém II Energy Generation S.A., Itaqui Energy Generation S.A., Parnaíba Energy Generation and Commercialization S.A. and Parnaíba II Energy Generation S.A.

Declarations

Conflict of interests No interests to declare.

References

1. Castro TL, Pereira MVS, Darwish FA (2021) On the influence of mean shear stress on multiaxial high cycle fatigue of metallic materials. Mater Res 24(1):20200319. https://doi.org/10.1590/1980-5373-MR-2020-0319
2. Matake T (1977) Explanation on fatigue limit under combined stress. Bull JSME 20(141):257–264. https://doi.org/10.1299/jsme1958.20.257
3. Susmel L, Lazzarin P (2002) A bi-parametric Wöhler curve for high cycle multiaxial fatigue assessment. Fatigue Fract Eng Mater Struct 25(1):63–78. https://doi.org/10.1046/j.1460-2695.2002.00462.x
4. Findley WN (1959) A theory for the effect of mean stress on fatigue of metals under combined torsion and axial load or bending. J Eng Ind 81(4):301–305. https://doi.org/10.1115/1.4008327
5. Carpinteri A, Spagnoli A (2001) Multiaxial high-cycle fatigue criterion for hard metals. Int J Fatigue 23(2):135–145. https://doi.org/10.1016/S0142-1123(00)00075-X
6. Liu Y, Mahadevan S (2005) Multiaxial high-cycle fatigue criterion and life prediction for metals. Int J Fatigue 27(7):790–800. https://doi.org/10.1016/j.ijfatigue.2005.01.003
7. Papadopoulos IV, Davoli P, Gorla C, Filippini M, Bernasconi A (1997) A comparative study of multiaxial high-cycle fatigue criteria for metals. Int J Fatigue 19(3):219–235. https://doi.org/10.1016/S0142-1123(96)00064-3
8. Garud YS (1981) Multiaxial fatigue: a survey of the state-of-the-art. J Test Eval 9(3):165–178
9. Wang YY, Yao WX (2004) Evaluation and comparison of several multiaxial fatigue criteria. Int J Fatigue 26(1):17–25. https://doi.org/10.1016/S0142-1123(03)00110-5
10. You BR, Lee SB (1996) A critical review on multiaxial fatigue assessments of metals. Int J Fatigue 18(4):235–244. https://doi.org/10.1016/0142-1123(96)00002-3
11. Castro TL, Araujo LC, Pereira MV, Darwish FA, da Silva GA, Araújo JA (2023) Evaluation of finite high cycle fatigue life of hard steels using the elliptical curve method. Fatigue Fract Eng Mater Struct. https://doi.org/10.1111/ffe.14101
12. Zenner H, Heidenreich R, Richter I (1985) Dauerschwingfestigkeit bei nichtsynchroner mehrachsiger Beanspruchung. Materwiss Werksttech. https://doi.org/10.1002/mawe.19850160310
13. Nishihara T, Kawamoto M (1945) The Strength of metals under combined alternating bending and torsion with phase difference. Mem Coll Eng, Kyoto Imp Univ 11(5):85–112
14. Froustey C, Lasserre S (1989) Multiaxial fatigue endurance of 30NCD16 steel. Int J Fatigue. https://doi.org/10.1016/0142-1123(89)90436-2
15. Carpinteri A, Spagnoli A, Vantadori S, Bagni C (2013) Structural integrity assessment of metallic components under multiaxial fatigue: the C-S criterion and its evolution. Fatigue Fract Eng Mater Struct 36(9):870–883. https://doi.org/10.1111/ffe.12037
16. McDiarmid DL (1987) Fatigue under out-of-phase bending and torsion. Fatigue Fract Eng Mater Struct 9(6):457–475. https://doi.org/10.1111/j.1460-2695.1987.tb00471.x
17. Carpinteri A, Brighenti R, Spagnoli A (2000) Fracture plane approach in multiaxial high-cycle fatigue of metals. Fatigue Fract

Eng Mater Struct 23(4):355–364. https://doi.org/10.1046/J.1460-2695.2000.00265.X